Proceedings of the ASME 2014 International Design Engineering Technical Conferences & Computers and Information in Engineering Conference
IDETC/CIE 2014
August 17-August 20, 2014, BUFFALO,NEW YORK, USA

DETC2014-35340

THEORETICAL MODELING OF A PRESSURE-OPERATED SOFT SNAKE ROBOT

Ming Luo
Robotics Engineering
Worcester Polytechnic Institute
Worcester, MA 01609
School of Computer and Information
AnQing Normal University
Anqing, Anhui 246011, China
Email: mluo@wpi.edu

Mahdi Agheli*
Cagdas D. Onal
Mechanical Engineering
Worcester Polytechnic Institute
Worcester, MA 01609
Email address:mmaghelih,cdonal@wpi.edu

ABSTRACT

This paper addresses the theoretical modeling of the dynamics of a pressure-operated soft snake robot. An accurate dynamic model is a fundamental requirement for optimization, control, navigation, and learning algorithms for a mobile robot that can undergo serpentine locomotion. Such algorithms can be readily implemented for traditional rigid robots, but remain a challenge for nonlinear and low-bandwidth soft robotic systems. A framework to solve the 2-D modeling problem of a soft robotic snake is detailed with a general approach applicable to most pressure-operated soft robots that are developed by a modular kinematic arrangement of bending-type fluidic elastomer actuators. The model is simulated using measured physical parameters of the robot and workspace. The theoretical results are verified through a proof-of-concept comparison to locomotion experiments on a flat surface with measured frictional properties. Experimental results indicate that the proposed model describes the motion of the robot.

INTRODUCTION

Robots promise to improve our lives in search and rescue applications. These applications require special robotic capabilities that may not be fulfilled by traditional mobile robots such as operating through narrow openings or complex passages. For such conditions, a robotic snake is a suitable candidate since it can navigate on unstructured terrain without limbs while being able to pass through narrow space similar to its biological counterpart.

Many researchers analyzed the principles of snake locomotion and developed robotic equivalents that can replicate snake motion. The first snake robot was developed by Shigeo Hirose at Tokyo Institute of Technology in 1971 [1]. During 40 years of research since, many snake robots have been developed, including Anna Konda, a large firefighting snake, Aiko, a portable system for experimentation, and Pneumosnake, developed to investigate joint actuation based on pneumatic bellows [2]. Recent research on the snake inspired robots for the minimally invasive surgery application [3], the snake robot can work on a step environment [4].

On the other hand, current snake robots do not utilize body flexibility. Since traditional robot fabrication is based on rigid links, robotic snakes may not be as safe and adaptive as their natural counterparts. Our objective in this research is to develop a pneumatically actuated soft robotic snake that can overcome the limitations of rigid snake robots. Soft robotics has recently seen a flurry of research including many different kinds of crawling robots [5–7].

The first generation of our soft snake robot was developed in [8] and [9]. The body is fabricated by molding in three layers. The total manufacturing and assembly process takes 14 hours

*Address all correspondence to this author.

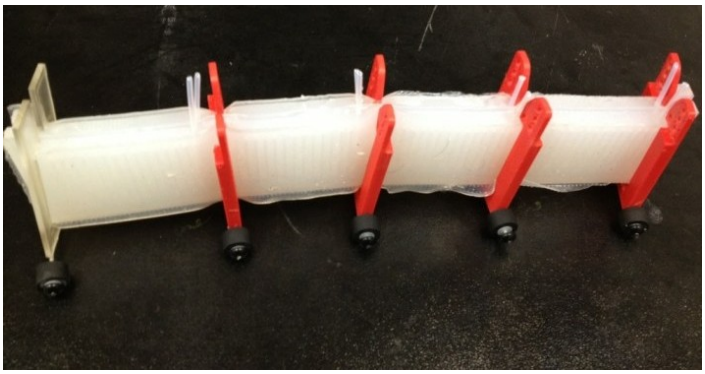

FIGURE 1. Experimental prototype of our pressure-operated soft robotic snake.

from scratch, resulting in an inexpensive robot. A recent prototype of our fluidic soft robot is shown in Fig. 1. Some challenges with the first iteration of the snake robot included the need for an accurate model for deeper research, a perception system for gait control, and a skin that offers anisotropic friction to eliminate the passive wheels, a current problem in snake robots in general.

This paper focuses on the first challenge. Snake robot modeling is a mature discipline for rigid robots. [10] and [11] study modeling a rigid snake robot in 2-D. [12] add expressions for the linear velocity of individual links based on previous work and divide the general model into an actuated and an un-actuated part. Subsequently, partial feedback linearization of the model is presented. In addition, [12] proposes a simplified model after linearization and gives proofs of stability and controllability of a rigid snake robot based on the proposed model. On the other hand, [13–15] study segmented rigid snake robot modeling in 3-D by taking vertical motions into account.

However, there exists limited mathematical modeling studies for soft robots since the deformable nature of such systems creates a challenge, such that a soft body may create infinite degrees of freedom. In previous work, we utilized a fundamental constant curvature kinematic model and augmented an anisotropic friction function to iteratively describe the shape of the body over time and provide intuition about the locomotion of our soft snake robot [9]. In this work, we treat each soft segment as a joint and analyze short rigid connectors as links. This approach is compatible with existing rigid snake robot kinematics modeling studies and provides a more accurate description of the whole system.

The outline of the paper is as follows: Section II shows the mathematical details of the soft snake robot model, Section III displays the dynamic simulation studies of a simplified model. Section IV describes the fabrication of the robot, the experimental setup and results. Section V concludes the paper and discusses potential future research directions.

TABLE 1. Parameters of the Soft Robotic Snake Model

Symbol	Description
N	Number of links
l_1	Half the length of the rigid link
l_2	The length of the soft segment
m	Mass of each link (including passive wheels)
J	Moment of inertia of each link
ΔS	The cross section of the soft actuator
U_t	The friction factor in the tangential direction
U_n	The friction factor in the normal direction
$\boldsymbol{\theta} \in \mathbb{R}^N$	Link global orientation vector
$\boldsymbol{\kappa} \in \mathbb{R}^{N-1}$	Segment curvature vector
$\boldsymbol{X}, \boldsymbol{Y} \in \mathbb{R}^N$	Link CoM global coordinates vector
(p_x, p_y)	Global coordinates of the CoM of the robot
$\boldsymbol{P} \in \mathbb{R}^{N-1}$	Segment pressure input vector
$\boldsymbol{f}_{R,x}, \boldsymbol{f}_{R,y} \in \mathbb{R}^N$	Ground friction force vectors
$\boldsymbol{h}_x, \boldsymbol{h}_y \in \mathbb{R}^{N-1}$	Joint constraint force vectors

0.1 Complete Model

This section proposes a model of the soft snake robot. A general soft snake robot comprises N rigid links of length $2l_1$ and $N-1$ soft segments of length l_2. All N links have the same moment of inertia J and mass m. We assume that the link center of mass is located at the geometric center of each link. Table I lists all the mathematical parameters of the kinematics and dynamics model, which are graphically depicted in Fig. 2.

The soft snake robot works on a 2-D surface. The following definitions are illustrated similar to a rigid snake robot [12]:

Definition 1 (Link angle) The link angle of link $i \in (1,...,N)$ of the snake robot is noted by $\theta_i \in \mathbb{R}$ with respect to the global x axis with counterclockwise positive direction.

Definition 2 (Curvature) The curvature of joint $i \in (1,...,N-1)$ of the snake robot is noted by $\kappa_i \in \mathbb{R}$ is defined as:

$$\kappa_i = \frac{\theta_i - \theta_{i+1}}{l_2} \tag{1}$$

Definition 3 (The global position) The position of the robot with respect to the global frame $\boldsymbol{p} \in \mathbb{R}^2$ The vector $\boldsymbol{X} = \begin{pmatrix} x_1 , \ldots , x_N \end{pmatrix}^T \in \mathbb{R}^N$ $\boldsymbol{Y} = \begin{pmatrix} y_1 , \ldots , y_N \end{pmatrix}^T \in \mathbb{R}^N$ $\boldsymbol{e} = \begin{pmatrix} 1 , \ldots , 1 \end{pmatrix}^T \in \mathbb{R}^N$

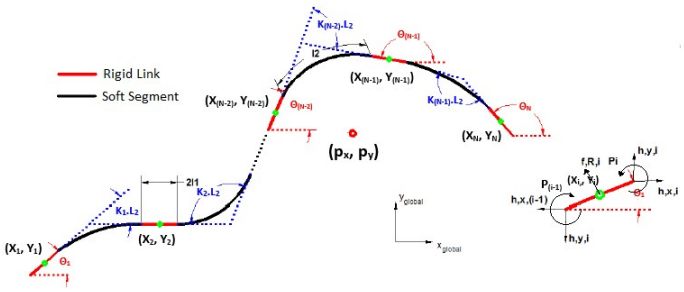

FIGURE 2. The complete model of a soft robotic snake.

$$\boldsymbol{p} = \begin{pmatrix} p_x \\ p_y \end{pmatrix} = \begin{pmatrix} \frac{1}{Nm}\sum_{i=1}^{N} m x_i \\ \frac{1}{Nm}\sum_{i=1}^{N} m y_i \end{pmatrix} = \frac{1}{N}\begin{pmatrix} \boldsymbol{e}^T\boldsymbol{X} \\ \boldsymbol{e}^T\boldsymbol{Y} \end{pmatrix} \tag{2}$$

The position difference between two neighbor links has two parts: The rigid link and the soft segment. So the position relationship of all links $i \in (1, ..., N-1)$

$$\begin{aligned} \boldsymbol{DX} + l_1\boldsymbol{A}cos\boldsymbol{\theta} + l_2\boldsymbol{diag}(\boldsymbol{D}sin\boldsymbol{\theta})\overline{\kappa} = \boldsymbol{0} \\ \boldsymbol{DY} + l_1\boldsymbol{A}sin\boldsymbol{\theta} - l_2\boldsymbol{diag}(\boldsymbol{D}cos\boldsymbol{\theta})\overline{\kappa} = \boldsymbol{0}. \end{aligned} \tag{3}$$

The vectors $\boldsymbol{A} = \begin{pmatrix} 1 & 1 & & \\ & \ddots & & \\ & & \ddots & \\ & & 1 & 1 \end{pmatrix} \in \mathbb{R}^{(N-1)\times N}$,

$\boldsymbol{D} = \begin{pmatrix} 1 & -1 & & \\ & \ddots & & \\ & & \ddots & \\ & & 1 & -1 \end{pmatrix} \in \mathbb{R}^{(N-1)\times N}$, and

$\overline{\kappa} = \left(\frac{1}{\kappa_1}, \ldots, \frac{1}{\kappa_{N-1}}\right)^T \in \mathbb{R}^{N-1}$. Combining equations (2) and (3), the center position of each link is given as:

$$\begin{aligned} \boldsymbol{X} &= -l_1\boldsymbol{K}^T cos\boldsymbol{\theta} - l_2\boldsymbol{Z}\boldsymbol{diag}(\boldsymbol{D}sin\boldsymbol{\theta})\overline{\kappa} + \boldsymbol{e}p_x \\ \boldsymbol{Y} &= -l_1\boldsymbol{K}^T sin\boldsymbol{\theta} + l_2\boldsymbol{Z}\boldsymbol{diag}(\boldsymbol{D}cos\boldsymbol{\theta})\overline{\kappa} + \boldsymbol{e}p_y, \end{aligned} \tag{4}$$

where $\boldsymbol{Z} = \boldsymbol{D}^T(\boldsymbol{D}\boldsymbol{D}^T)^{-1} \in \mathbb{R}^{N\times N-1}$, and
$\boldsymbol{K} = \boldsymbol{A}^T(\boldsymbol{D}\boldsymbol{D}^T)^{-1}\boldsymbol{D} \in \mathbb{R}^{N\times N}$.

The soft snake robot can undulate forward with the help of ground friction forces. In this work we use Coulomb friction model as:

$$\begin{aligned} \boldsymbol{f_R} &= \begin{pmatrix} \boldsymbol{f}_{R,x} \\ \boldsymbol{f}_{R,y} \end{pmatrix} \\ &= -mg\begin{pmatrix} U_t\boldsymbol{C}_\theta & -U_n\boldsymbol{S}_\theta \\ U_t\boldsymbol{S}_\theta & -U_n\boldsymbol{C}_\theta \end{pmatrix} sgn\left(\begin{pmatrix} \boldsymbol{C}_\theta & \boldsymbol{S}_\theta \\ -\boldsymbol{S}_\theta & \boldsymbol{C}_\theta \end{pmatrix}\begin{pmatrix} \dot{\boldsymbol{X}} \\ \dot{\boldsymbol{Y}} \end{pmatrix}\right), \end{aligned} \tag{5}$$

where $\boldsymbol{S}_\theta = diag(sin\boldsymbol{\theta}) \in \mathbb{R}^{N\times N}$, and
$\boldsymbol{C}_\theta = diag(cos\boldsymbol{\theta}) \in \mathbb{R}^{N\times N}$

Fig. 2 depicts the force balance on each link. The ground friction force and joint constraint force both have influence on the dynamics of the soft snake robot. According to the Newton's law, the force balance equations are given as:

$$\begin{aligned} m\ddot{\boldsymbol{X}} &= \boldsymbol{f}_{R,x} + \boldsymbol{D}^T\boldsymbol{h}_x, \\ m\ddot{\boldsymbol{Y}} &= \boldsymbol{f}_{R,y} + \boldsymbol{D}^T\boldsymbol{h}_y, \end{aligned} \tag{6}$$

where $\boldsymbol{h_x} = \left(h_{x,1} \ \ldots, h_{x,N}\right)^T \in \mathbb{R}^N$,
$\boldsymbol{h_y} = \left(h_{y,1} \ \ldots, h_{y,N}\right)^T \in \mathbb{R}^N$

Similarly, the torque balance for all links is given as:

$$J\ddot{\boldsymbol{\theta}} = \Delta Sl_2\boldsymbol{D}^T\boldsymbol{P} - l_1\boldsymbol{S}_\theta\boldsymbol{A}^T\boldsymbol{h_x} + l_1\boldsymbol{C}_\theta\boldsymbol{A}^T\boldsymbol{h_y}. \tag{7}$$

Taking the first and second derivatives of (4), we can plug expressions into (5) and (6) and finally combine (7) to yield:

$$\begin{aligned} &\boldsymbol{M}_\theta\ddot{\boldsymbol{\theta}} + \boldsymbol{W}\dot{\boldsymbol{\theta}}^2 + \boldsymbol{T}\dot{\boldsymbol{\theta}} + \boldsymbol{Y}\ddot{\boldsymbol{k}} + \boldsymbol{Q} - l_1\boldsymbol{S}_\theta\boldsymbol{K}\boldsymbol{f}_{R,x} + l_1\boldsymbol{C}_\theta\boldsymbol{K}\boldsymbol{f}_{R,y} = \Delta Sl_2\boldsymbol{D}^T\boldsymbol{P} \\ &N\ddot{m}\dot{\boldsymbol{P}} = \boldsymbol{E}^T\boldsymbol{f_R}, \end{aligned} \tag{8}$$

where

$$\boldsymbol{M}_\theta = \boldsymbol{J}\boldsymbol{I}_N + ml_1^2\boldsymbol{S}_\theta\boldsymbol{V}\boldsymbol{S}_\theta + ml_1^2\boldsymbol{C}_\theta\boldsymbol{V}\boldsymbol{C}_\theta - ml_1l_2\boldsymbol{S}_\theta\boldsymbol{Z}\boldsymbol{B_1} - ml_1l_2\boldsymbol{C}_\theta\boldsymbol{Z}\boldsymbol{B_2} \tag{9}$$

$$\boldsymbol{W}_\theta = ml_1^2\boldsymbol{S}_\theta\boldsymbol{V}\boldsymbol{C}_\theta - ml_1^2\boldsymbol{C}_\theta\boldsymbol{V}\boldsymbol{S}_\theta - ml_1l_2\boldsymbol{S}_\theta\boldsymbol{Z}\boldsymbol{B_2} + ml_1l_2\boldsymbol{C}_\theta\boldsymbol{Z}\boldsymbol{B_1} \tag{10}$$

$$\boldsymbol{T}_\theta = -ml_1l_2\boldsymbol{S}_\theta\boldsymbol{Z}\boldsymbol{B_5} - ml_1l_2\boldsymbol{C}_\theta\boldsymbol{Z}\boldsymbol{B_8} \tag{11}$$

$$\boldsymbol{Q}_\theta = -ml_1l_2\boldsymbol{S}_\theta\boldsymbol{Z}\boldsymbol{B_5} - ml_1l_2\boldsymbol{C}_\theta\boldsymbol{Z}\boldsymbol{B_8} \tag{12}$$

$$\boldsymbol{Y}_\theta = -ml_1l_2\boldsymbol{S}_\theta\boldsymbol{Z}\boldsymbol{B_6} - ml_1l_2\boldsymbol{C}_\theta\boldsymbol{Z}\boldsymbol{B_9} \tag{13}$$

for vectors:
$\boldsymbol{V} = \boldsymbol{A}^T(\boldsymbol{D}\boldsymbol{D}^T)^{-1}\boldsymbol{A} \in \mathbb{R}^{N\times N}$
$\boldsymbol{E} = \begin{pmatrix} \boldsymbol{e} & \boldsymbol{0}_{N\times 1} \\ \boldsymbol{0}_{N\times 1} & \boldsymbol{e} \end{pmatrix} \in \mathbb{R}^{2N\times 2}$
Equations (14),(15) and (67) describe the format of the matrices B_1 to B_9 for the given $C_{j,k}$ elements for each case.
$\boldsymbol{B_1} = \boldsymbol{F_1}$ with $C_{1,2i-1} = \frac{cos\theta_i}{\kappa_i}$ and $C_{1,2i} = -\frac{cos\theta_{i+1}}{\kappa_i}$
$\boldsymbol{B_2} = \boldsymbol{F_1}$ with $C_{1,2i-1} = -\frac{sin\theta_i}{\kappa_i}$ and $C_{1,2i} = \frac{sin\theta_{i+1}}{\kappa_i}$
$\boldsymbol{B_3} = \boldsymbol{F_1}$ with $C_{1,2i-1} = -\frac{\kappa_i^2 cos\theta_i}{\dot{\kappa_i}}$ and $C_{1,2i} = \frac{\kappa_i^2 cos\theta_{i+1}}{\dot{\kappa_i}}$
$\boldsymbol{B_4} = \boldsymbol{F_2}$ with $C_{2,i} = \frac{\dot{\kappa_i}^2(sin\theta_i - sin\theta_{i+1})}{\kappa_i^3}$
$\boldsymbol{B_5} = \boldsymbol{F_3}$ with $C_{3,i} = \frac{sin\theta_{i+1} - sin\theta_i}{\kappa_i^2}$
$\boldsymbol{B_6} = \boldsymbol{F_1}$ with $C_{1,2i-1} = \frac{\kappa_i \dot{sin}\theta_i}{\kappa_i^2}$ and $C_{1,2i} = -\frac{\kappa_i \dot{sin}\theta_{i+1}}{\kappa_i^2}$

$\boldsymbol{B_7} = \boldsymbol{F_2}$ with $C_{2,i} = \frac{\dot{k_i}^2(cos\theta_i - cos\theta_{i+1})}{\kappa_i^3}$

$\boldsymbol{B_8} = \boldsymbol{F_3}$ with $C_{3,i} = \frac{cos\theta_{i+1} - cos\theta_i}{\kappa_i^2}$

$$\boldsymbol{F_1} = \begin{pmatrix} \mathbf{0}_{0\times0} & C_{1,1} & C_{1,2} & \mathbf{0}_{1\times N-2} \\ \mathbf{0}_{1\times1} & C_{1,3} & C_{1,4} & \mathbf{0}_{1\times N-3} \\ \vdots & \vdots & \vdots & \vdots \\ \mathbf{0}_{1\times N-3} & C_{1,2N-5} & C_{1,2N-4} & \mathbf{0}_{1\times1} \\ \mathbf{0}_{1\times N-2} & C_{1,2N-3} & C_{1,2N-2} & \mathbf{0}_{0\times0} \end{pmatrix} \in \mathbb{R}^{(N-1)\times N} \quad (14)$$

$$\boldsymbol{F_2} = 2\begin{pmatrix} C_{2,1} \\ C_{2,2} \\ \vdots \\ C_{2,N-2} \\ C_{2,N-1} \end{pmatrix} \in \mathbb{R}^{(N-1)\times1} \quad (15)$$

$$\boldsymbol{F3} = \begin{pmatrix} \mathbf{0}_{0\times0} & C_{3,1} & \mathbf{0}_{1\times N-1} \\ \mathbf{0}_{1\times1} & C_{3,2} & \mathbf{0}_{1\times N-2} \\ \vdots & \vdots & \vdots \\ \mathbf{0}_{1\times N-2} & C_{3,N-2} & \mathbf{0}_{1\times1} \\ \mathbf{0}_{1\times N-1} & C_{3,N-1} & \mathbf{0}_{0\times0} \end{pmatrix} \in \mathbb{R}^{(N-1)\times N}. \quad (16)$$

These set of equations provide an accurate mathematical representation of the dynamics of our soft snake robot. However, they are difficult to implement in a simulated environment. Compared with a rigid snake model, the complicated geometry of a soft snake is associated with significant computational cost, which also makes the complete model not ideal for model based control approaches. In what follows, we describe a simplification that leads to more tractable expressions.

0.2 Simplified model for simulation

In the previous section, we described a complete dynamic model of a soft snake robot, resulting in complicated series of expressions. For simplicity and practical applications, the rigid link lengths (l_1) can be ignored as compared to the length of the soft segments (l_2). Fig. 3 displays a simplified dynamics modeling approach for a fluidic soft snake robot graphically.

With the zero link length assumption, the position relationship for all links in (3) becomes:

$$\begin{aligned} \boldsymbol{DX} + l_2\boldsymbol{diag}(\boldsymbol{D}sin\boldsymbol{\theta})\overline{\kappa} = \mathbf{0}, \\ \boldsymbol{DY} - l_2\boldsymbol{diag}(\boldsymbol{D}cos\boldsymbol{\theta})\overline{\kappa} = \mathbf{0}. \end{aligned} \quad (17)$$

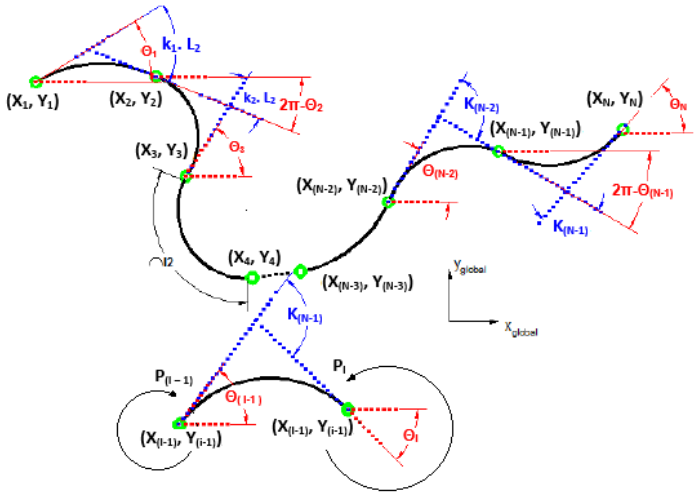

FIGURE 3. The simple model

The center position of links equation (5=4) becomes:

$$\begin{aligned} \boldsymbol{X} = -l_2\boldsymbol{Z}\boldsymbol{diag}(\boldsymbol{D}sin\boldsymbol{\theta})\overline{\kappa} + \boldsymbol{ep_x}, \\ \boldsymbol{Y} = l_2\boldsymbol{Z}\boldsymbol{diag}(\boldsymbol{D}cos\boldsymbol{\theta})\overline{\kappa} + \boldsymbol{ep_y}. \end{aligned} \quad (18)$$

The simplified model of the soft snake robot has no rigid links, so in equation (7), the joint constraint force term can be ignored, because the l_1 is 0 as:

$$\boldsymbol{J}\ddot{\boldsymbol{\theta}} = \boldsymbol{\Delta S} l_2 \boldsymbol{D}^T \boldsymbol{P}. \quad (19)$$

The combined dynamic motion expression (8) becomes:

$$\begin{aligned} \boldsymbol{M}_\theta\ddot{\boldsymbol{\theta}} = \boldsymbol{\Delta S} l_2 \boldsymbol{D}^T \boldsymbol{P} \\ \boldsymbol{N}m\ddot{\boldsymbol{P}} = \boldsymbol{E}^T \boldsymbol{f}_{\boldsymbol{R}}, \end{aligned} \quad (20)$$

where $\boldsymbol{M}_\theta = \boldsymbol{J}\boldsymbol{I}_N$

Equation (20) shows the soft snake robot system as a whole. Next step is separating the actuated and un-actuated dynamics for the following deeper analysis. Defining:

$$\begin{aligned} \boldsymbol{q}_\kappa = \begin{pmatrix} \kappa^* \\ \boldsymbol{p} \end{pmatrix} \in \mathbb{R}^{N+2}, \\ \boldsymbol{\theta} = \boldsymbol{H}\boldsymbol{\kappa}^*, \end{aligned} \quad (21)$$

where

$\boldsymbol{\kappa}^* = \begin{pmatrix} \kappa_1 & , \ldots , & \kappa_{N-1} & \theta_N \end{pmatrix}^T \in \mathbb{R}^N,$

$$\boldsymbol{H} = \begin{pmatrix} 1 & 1 & 1 & \cdots & 1 & 1 \\ 0 & 1 & 1 & \cdots & 1 & 1 \\ \vdots & & & & & \vdots \\ 0 & 0 & 0 & \cdots & 0 & 1 \end{pmatrix} \in \mathbb{R}^{N \times N}.$$

Inserting (21) into (20), and pre-multiplying with H^T yields:

$$\boldsymbol{M}^*_{\kappa^*}\ddot{\boldsymbol{q}}_{\boldsymbol{\kappa}} + \boldsymbol{G}^*_{\kappa^*}\boldsymbol{f}_{\boldsymbol{R}} = \Delta \boldsymbol{S} l_2 \overline{B} \boldsymbol{P}, \tag{22}$$

where

$$\boldsymbol{M}^*_{\kappa^*} = \begin{pmatrix} \boldsymbol{H}^T \boldsymbol{M}_{\boldsymbol{\theta}}(\boldsymbol{\kappa}^*) & \boldsymbol{0}_{N\times 2} \\ \boldsymbol{0}_{2\times N} & NM\boldsymbol{I}_2 \end{pmatrix}$$

$$\boldsymbol{G}^*_{\kappa^*} = \begin{pmatrix} \boldsymbol{0}^{1\times N} & \boldsymbol{0}^{1\times N} \\ -\boldsymbol{e}^T & \boldsymbol{0}^{1\times N} \\ \boldsymbol{0}^{1\times N} & -\boldsymbol{e}^T \end{pmatrix}$$

$$\overline{B} = \begin{pmatrix} \boldsymbol{I}_{N-1} \\ \boldsymbol{0}^{3\times N-1} \end{pmatrix}$$

1 Results

To verify our modeling approach we first developed simulations of the simplified soft snake robot dynamic model. The simulations adopt the ODE toolbox in Matlab to solve the differential equations of the soft snake robot model. Beside the snake robot's system dynamics, the model reflects the dynamic response of the fluidic elastomer actuators used as segments in our robot as shown in Fig. 4, [8, 9, 16].

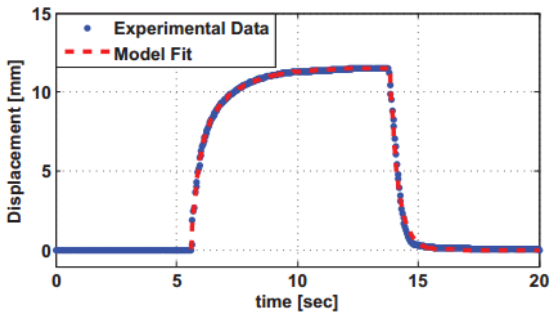

FIGURE 4. Dynamic response of the fluidic elastomer actuators under step pressure inputs [9].

Fig. 5(a) displays simulation results including the initial and final positions of the whole snake as well as the trajectory of the head. The following set of parameters were used in these simulations: $N = 5$, $l_2 = 0.055$ m, $m = 0.1$ kg, $U_t = 0.0966$, $U_n = 0.68$, pressure $= 5$ psi, frequency $= 1/3$ hz. Fig. 5(b) displays the position and velocity of the center of mass of the soft snake robot for the same simulation.

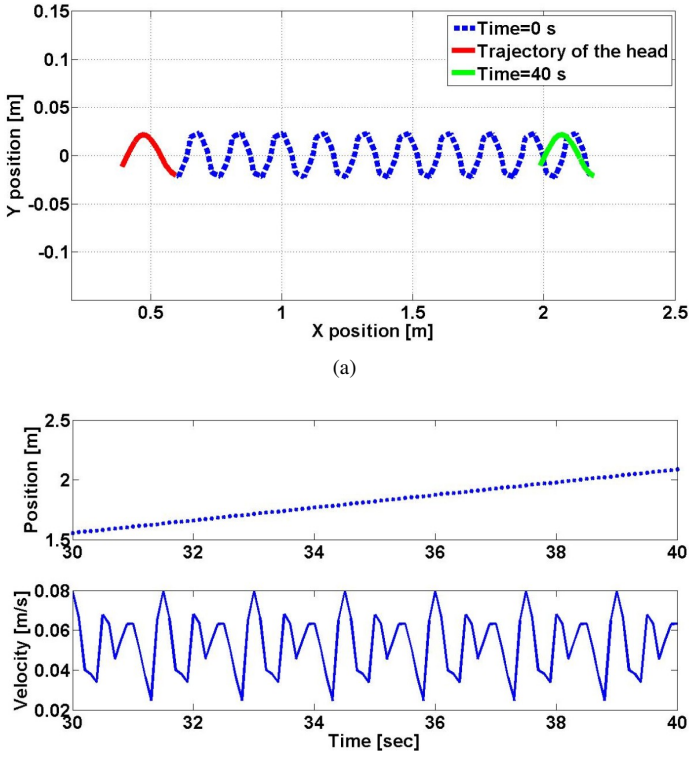

FIGURE 5. Dynamic model simulation of the soft snake robot.

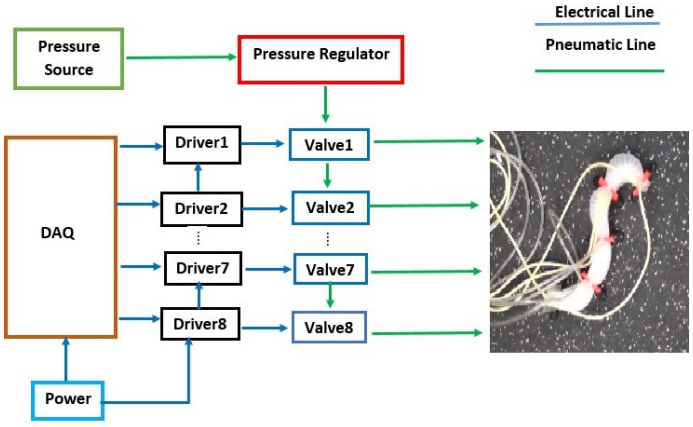

FIGURE 6. The experimental system.

The fabrication process of the soft snake robot can be divided into three steps [8]:

Step 1 Draw and 3-D print three pre-molds of the soft snake body. Two premolds carry the negative of parallel rectangular fluidic channels connected on both ends in a serpentine arrangement. The other one has a thin rectangular opening,

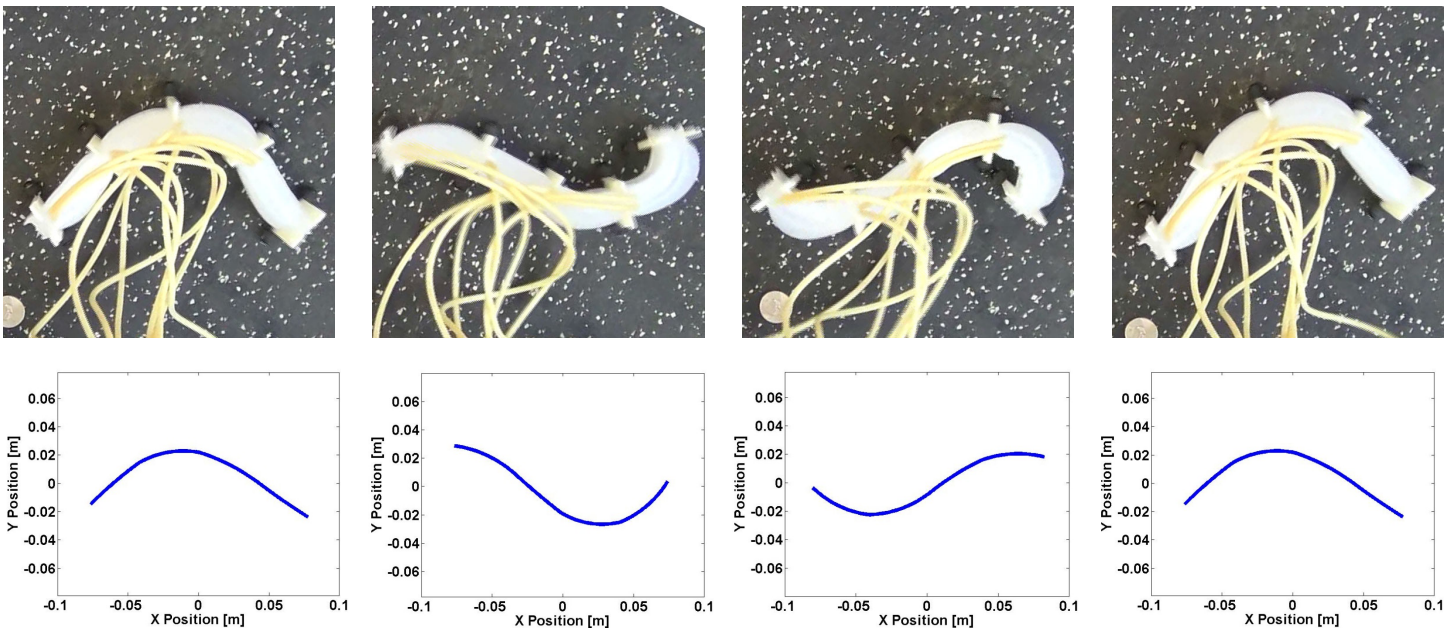

(a) $t = 0$ s (b) $t = 1$ s (c) $t = 2$ s (d) $t = 3$ s

FIGURE 7. Comparison of the snake robot shapes between the simulation and the experiment at 0,1,2 and 3 s.

with the same length and width as the channel layer.

Step 2 Embed an inextensible flexible sheet on the second mold, in order to add a constraint for the soft body to undergo bending deformation upon pressurization. Then pour silicone rubber into both premolds.

Step 3 When cured, remove the three molds and bond two channel molds on both sides of the constraint mold using thin layers of uncured silicone rubber as glue.

The fluidic sub-system, the control sub-system, and the robot itself form the whole soft snake robot system as depicted in Fig. 6. As a fluid source, we use a shop air nozzle that can provide a large pressure input, which passes through a regulator to obtain controlled pressure values more compatible with our actuators, typically below 5 psi. The regulated pressure input is connected to a valve array that drives the soft snake robot. Each segment of the robot requires two valves to achieve bidirectional bending. The aim of the control system is to move the snake robot in a way that follows the serpentine gait [9]. A NI-DAQ PCI 6009 transfers commands from Matlab to drive each valve. Eight digital outputs of the NI-6009 are used to control eight miniature solenoid valves, turning them on or off.

In order to verify the model, the value of some parameters of the snake robot itself and the workspace should be determined. Table II displays a list of measured parameters. We used a spring scale to measure the values of friction factors in two different directions by recording the force from the spring scale as the robot began to move upon horizontal pulling. In addition, in order to measure the sliding friction in the normal direction, the passive wheels of the snake were fixed before the measurement. We performed ten measurements for both the tangential rolling friction and normal sliding friction cases. The mean friction coefficient values in tangential and normal directions were 0.0966 and 0.68, respectively, with standard deviations of 0.0015 and 0.01.

TABLE 2. Experimental Parameters

Symbol	Description	Value	Unit
N	Number of segments	5	
G	Weight of each soft segment	0.25	kg
U_t	The tangential friction factor	0.0966	
U_n	The normal friction factor	0.68	
P_{max}	Maximum input pressure	5	psi

For our pressure-operated actuators the input pressure is usually below 5 psi. We captured snapshots of the snake motion experimentally when the undulation frequency is 0.33 Hz at four time steps and compared with simulation results in Fig. 7. Figures 8 and 9 show the center of mass (CoM) velocity of the snake from experiments and simulations for varying frequency and pressure values. Compared to the experimental results, the red curves fit the body motion of the snake robot prototype reasonably well. From Fig 8, the optimal frequency is around

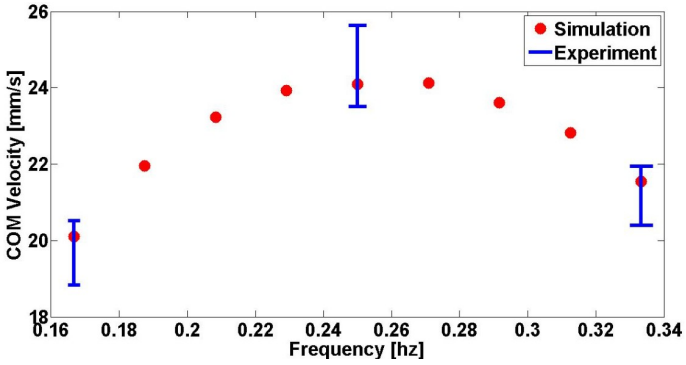

FIGURE 8. Comparison of the CoM velocity of the snake between the experimental and simulation results at different frequencies when the pressure is fixed at 4.5 psi. Blue errorbars represent the experimental results and the red dots are the simulation results. The experimental data contained three runs at each frequency: $1/6$, $1/4$, and $1/3$ Hz.

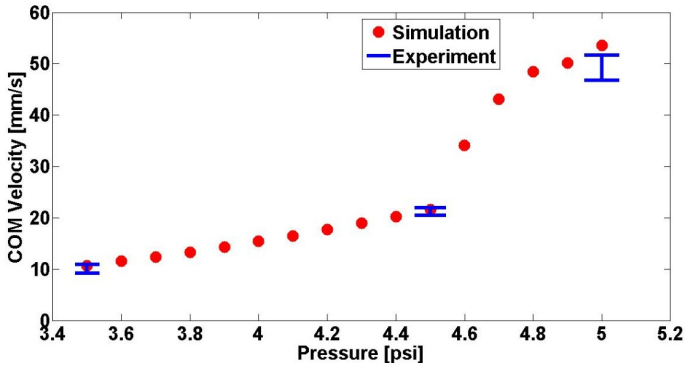

FIGURE 9. Comparison of the CoM velocity of the snake between the experimental and simulation results at different pressure values when the frequency is fixed at $1/3$ Hz. Blue errorbars represent the experimental results and the red dots are the simulation results. The experimental data contained three runs at each pressure value: 3.5, 4.5, and 5 psi.

0.25 Hz. If the frequency is lower, the pressure-on and pressure-release periods are unnecessarily large, so the snake spends more energy in bending its segments, instead of linear motion. If the frequency is higher, the pressure-on time and the pressure-release time are smaller, and the soft segment cannot bend and generate enough torque, which makes the linear motion slower. From Fig. 9, the CoM velocity grows as the input pressure value increases when the frequency is 0.33 Hz.

From Figs. 7, 8, and 9, some errors exist between simulations and experiments. Besides the errors resulting from small frictional differences on the ground, the biggest source of errors is the external tubing, which is required to transfer pressure to the fluidic actuation channels. While the robot is moving, the tubing was observed to exert forces on the robot due to stiffness and limited length, pulling the robot back and reducing velocity.

2 Conclusion

This paper presents a mathematical dynamic model of a soft snake robot made of silicone, provided simulation results, and verified the models effectiveness through a proof-of-concept comparison of the experimental results on the locomotion of the robot on a flat surface. The fundamental approach we take in this modeling study is applicable to most pressure-operated soft robots we develop by a modular kinematic arrangement of bending-type fluidic actuators embedded in the elastomer.

This work represents our first step to develop rigorous theoretical studies on fluidic elastomer robots. Based on the presented dynamic model, future studies on soft robots can implement advanced theoretical optimization, control, navigation, planning, and learning algorithms similar to their rigid counterparts.

Practically for low-level feedback control, the snake robot needs to measure its segment curvatures. Future work will focus on developing a soft curvature sensor compatible with our soft robot fabrication process. Another future goal is to eliminate the passive wheels which create the necessary frictional anisotropy required for serpentine locomotion. Most snake robots use this technique to slide on the ground more freely along the tangential axis than the normal axis. For real-world unstructured environments, wheels may not be the best solution. A soft robotic snake may be more suitable to eliminate wheels and use a skin similar to its natural counterpart due to its compliance and weight benefits. We aim to develop an artificial skin for the next generation of our soft snake robot.

Since a soft robot body is safer than a rigid one, our current work is suitable for search & rescue, medical, and manufacturing applications. The theoretical modeling study described in this paper will be extended to a 3-D workspace in order to move and control a 3-D soft manipulator towards the mentioned applications.

REFERENCES

[1] Hirose, S., 1993. *Biologically Inspired Robots: Snake-like Locomotors and Manipulators*. Oxford University Press.

[2] SINTEF.

[3] Ananthanarayanan, A., Bussemer, F., Gupta, S. K., and Desai, J. P., 2014. "Fabrication of highly articulated miniature snake robot structures using in-mold assembly of compliant joints". In Experimental Robotics, Springer, pp. 799–809.

[4] Tanaka, M., and Tanaka, K., 2013. "Climbing and descending control of a snake robot on step environments based on kinematics". In Intelligent Robots and Systems (IROS), 2013 IEEE/RSJ International Conference on, IEEE, pp. 3285–3290.

[5] Trimmer, B. A., Lin, H.-T., Baryshyan, A., Leisk, G. G., and Kaplan, D. L., 2012. "Towards a biomorphic soft robot: design constraints and solutions". In Biomedical Robotics

and Biomechatronics (BioRob), 2012 4th IEEE RAS & EMBS International Conference on, IEEE, pp. 599–605.

[6] Menciassi, A., Gorini, S., Pernorio, G., Weiting, L., Valvo, F., and Dario, P., 2004. "Design, fabrication and performances of a biomimetic robotic earthworm". In Robotics and Biomimetics, 2004. ROBIO 2004. IEEE International Conference on, IEEE, pp. 274–278.

[7] Morin, S. A., Shepherd, R. F., Kwok, S. W., Stokes, A. A., Nemiroski, A., and Whitesides, G. M., 2012. "Camouflage and display for soft machines". *Science,* ***337***(6096), pp. 828–832.

[8] Onal, C. D., and Rus, D., 2012. "A modular approach to soft robots". In Biomedical Robotics and Biomechatronics (BioRob), 2012 4th IEEE RAS & EMBS International Conference on, IEEE, pp. 1038–1045.

[9] Onal, C. D., and D.Rus, 2013. "Autonomous undulatory serpentine locomotion utilizing body dynamics of a fluidic soft robot". *Bioinspiration & biomimetics,* ***8***(2), p. 026003.

[10] Sato, M., Fukaya, M., and Iwasaki, T., 2002. "Serpentine locomotion with robotic snakes". *Control Systems, IEEE,* ***22***(1), pp. 64–81.

[11] Shugen, 2001. "Analysis of creeping locomotion of a snake-like robot". *Advanced Robotics,* ***15***(2), pp. 205–224.

[12] Pettersen, K. Y., Stavdahl, Ø., and Gravdahl, J. T., 2013. *Snake Robots: Modelling, Mechatronics, and Control*. Springer.

[13] Matsuno, F., and Suenaga, K., 2003. "Control of redundant 3d snake robot based on kinematic model". In Robotics and Automation, 2003. Proceedings. ICRA'03. IEEE International Conference on, Vol. 2, IEEE, pp. 2061–2066.

[14] Tanaka, M., and Matsuno, F., 2008. "Control of 3-dimensional snake robots by using redundancy". In Robotics and Automation, 2008. ICRA 2008. IEEE International Conference on, IEEE, pp. 1156–1161.

[15] Transeth, A. A., Leine, R. I., Glocker, C., and Pettersen, K. Y., 2008. "3-d snake robot motion: nonsmooth modeling, simulations, and experiments". *Robotics, IEEE Transactions on,* ***24***(2), pp. 361–376.

[16] Luo, M., Tao, W., Chen, F., Khuu, T. K., Ozel, S., and Onal, C. D., 2014. "Design improvements and dynamic characterization on fluidic elastomer actuators for a soft robotic snake". In 2014 IEEE Conference on Technologies for Practical Robot Applications (TePRA).